

# Supporting Information

## Synergistic Coordination in $^{89}\text{Zr}$ -DFO (Deferoxamine)

### Complexes: Computational and Experimental Insights into Auxiliary

### Ligands

Jiarui Li,<sup>‡a,b</sup> Chenghe Ding,<sup>‡c</sup> Yang Gao,<sup>\*a,b</sup> Lili Wen,<sup>b</sup> Pingping Zhao,<sup>a</sup> Zhou Lu,<sup>c</sup>  
Rui Luo,<sup>d</sup> Mingsong Shi,<sup>c</sup> Georg Schreckenbach,<sup>\*e</sup> Xiaoan Li,<sup>\*c,f</sup> Zhiming Wang<sup>a,b</sup>

- a. Institute of Fundamental and Frontier Sciences, University of Electronic Science and Technology of China, Chengdu, Sichuan 611731, China
- b. Shimmer Center, Tianfu Jiangxi Laboratory, Chengdu 641419, China
- c. NHC Key Laboratory of Nuclear Technology Medical Transformation, Mianyang Central Hospital, School of Medicine, University of Electronic Science and Technology of China, Mianyang, Sichuan, 621099, China
- d. Department of Nuclear Medicine, Mianyang Central Hospital, Mianyang 621000, China
- e. Department of Chemistry, University of Manitoba, Winnipeg, Manitoba R3T 2N2, Canada.
- f. Department of Gastroenterology, National Clinical Key Specialty, Mianyang Central Hospital, School of Medicine, University of Electronic Science and Technology of China, Mianyang 621000, China

\* Email : ygaoxs@gmail.com & ygaoxs@uestc.edu.cn (Y.G.) ;  
schrecke@cc.umanitoba.ca (G.S.) ; lixiaoan@sc-mch.cn (X.L.)

‡ These authors contributed equally to this work.

## Contents

Part 1. Methods .....	3
Part 2. Eight possible geometrical isomer structures of Zr <sup>IV</sup> -DFO .....	7
Part 3. Optimized geometries of the Zr <sup>IV</sup> -DFO-ligands complexes.....	8
Part 4. Geometric parameters of Zr <sup>IV</sup> -DFO-ligands complexes.....	11
Part 5. Comparison of Structural Parameters.....	12
Part 6. Optimized geometry of the [Zr <sup>IV</sup> (DFO)( <sup>in</sup> H <sub>2</sub> O)( <sup>out</sup> H <sub>2</sub> O)] <sup>+</sup> complex.....	14
Part 7. EDA-NOCV deformation densities $\Delta\rho$ of Zr <sup>IV</sup> -DFO-ligands complexes.....	15
Part 8. Stability Constants and Gibbs free energy.....	17
Part 9. The radiochemical purity of purified <sup>89</sup> Zr .....	18
Part 10. In vitro stability of [ <sup>89</sup> Zr]Zr-DFO and [ <sup>89</sup> Zr]Zr-DFO-ligands .....	19
Part 11. References.....	21

## Part 1. Methods

### Computational details

Because the Perdew-Burke-Ernzerhof (PBE)<sup>1</sup> functional can reasonably reproduce the results of high-level *ab initio* wave-function theory for Zr<sup>IV</sup>-DFO-ligands complexes,<sup>2, 3</sup> the spin-polarized generalized gradient approximation (GGA) with empirical dispersion<sup>4</sup> corrections, PBE-D3, was used throughout this work. Triple-zeta Slater-type basis sets<sup>5</sup> with two polarization functions (TZ2P) were used, with a [1s<sup>2</sup>-3d<sup>10</sup>] frozen core for Zr atom, a [1s<sup>2</sup>] frozen core for O, P and Cl atoms, and all electrons for H, C, N atoms, respectively. The scalar zeroth-order regular approximation (ZORA) was applied.<sup>6-9</sup> For all of the calculations, solvent effects were incorporated employing the conductor-like screening solvation model (COSMO) as an implicit solvation model using water as the solvent.<sup>10-13</sup> Since the Gibbs free energy for each complex was computed at 1 atm pressure, an entropy correction for higher pressure is a simple way to model translational degrees of freedom in the solvent. An effective pressure of  $p = 1354$  atm was used to mimic the condensed phase, which is the pressure obtained from  $p = \rho_w RT$ , corresponding to the experimental density of liquid water  $\rho_w = 997.02$  kg/ m<sup>3</sup> at the temperature of 298 K.<sup>14</sup>

The nature of the Zr<sup>IV</sup>-O<sub>DFO</sub> interactions has been investigated employing the EDA-NOCV method,<sup>15-18</sup> which combines the energy decomposition analysis (EDA) with the natural orbital for chemical valence (NOCV) approach. In the EDA method, the interaction energy  $\Delta E_{\text{int}}$  between the fragments is divided into four components:

$$\Delta E_{\text{int}} = \Delta E_{\text{elstat}} + \Delta E_{\text{Pauli}} + \Delta E_{\text{orb}} + \Delta E_{\text{disp}}$$

where the  $\Delta E_{\text{elstat}}$  term represents the quasi-classical electrostatic interaction between the unperturbed charge distributions of the prepared fragments, and the  $\Delta E_{\text{Pauli}}$  term is the electron-electron Pauli repulsion due to the orthogonality requirement of the orbitals. The  $\Delta E_{\text{orb}}$  term explains the process of forming covalent bonds through the inter-fragment mixing of the orbitals, and also explains the polarization within the fragments via intra-fragment orbital mixing. Finally, the  $\Delta E_{\text{disp}}$  term corresponds to the dispersion (van der Waals) interaction between the fragments. It should be noted that the use of the COSMO option with interacting fragments is not supported in the ADF program, so the EDA-NOCV calculations were performed under gas phase conditions i.e. gas phase EDA-NOCV analysis at the solution-optimized geometries. All calculations under gas-phase and aqueous solution conditions were spin restricted.

Geometry optimizations have been performed without imposing any symmetric constraints. The

optimized structures were analyzed with vibrational frequency calculations at the same level of theory to obtain thermochemical corrections as well as to ensure that all structures correspond to local minima. The calculations were performed using the Amsterdam Density Functional package (ADF 2017).<sup>19</sup>

**Theory for Calculating Stability Constants.** The simplest metal ligand complexation reaction is shown in the following equation.



The metal ion (M) undergoes a ligand replacement reaction with the ligand (L) in solution, leading to the releases of the solute ligand  $M(Sol)_m$  from the metal ion's coordination shell. The values of  $m$  and  $n$  represent the number of solvate ligands coordinated to the metal center and the denticity of the ligand, respectively. In the complexation reactions of the five complexes considered here, both  $m$  and  $n$  are 8. Since metal ions have multiple coordination sites, complexation reactions typically involve the binding of more than one ligand in a stepwise manner. The stability of the resulting complex is determined by the equilibrium constant (K), which is typically expressed as  $-\log K$  (pK). The individual equilibrium constant is multiplied together to yield the overall stability constant,  $\beta$ . When reporting stability constants, the number of metal ions and ligands involved in the reaction is usually indicated as a subscript. The complexation reaction of a metal ion with a ligand is denoted by  $\beta_{11}$ .

$$\log \beta_{11} = \log K = \log \frac{[ML(Sol)_{m-n}]}{[M(Sol)_m][L]} \approx \frac{\alpha_{ML(Sol)_{m-n}}}{\alpha_{M(Sol)_m} \alpha_L} = (\log_{10} e) \frac{-\Delta_r G}{RT} = \frac{-\Delta_r G}{2.303RT}$$

Where  $\Delta_r G$  represents the Gibbs free energy change of the reaction. The Gibbs free energy of the reaction is calculated as:

$$\Delta_r G = G(ML(Sol)_{m-n}) + nG(Sol) - G(M(Sol)_m) + G(L)$$

Thus, the stability constant ( $\log \beta$ ) is determined by the Gibbs free energy difference between the reactants and products.

## Experimental details

**Radio-thin layer chromatography (radio-TLC).** For the <sup>89</sup>Zr-DFO complexation assay, the water that has been treated by Chelex 100 sodium (Sigma-Aldrich, 11139-85-8) to remove trace metals was used to prepare a solution containing 2 M Na<sub>2</sub>CO<sub>3</sub> and 0.88 M Na<sub>2</sub>HPO<sub>4</sub>. For the complexation of <sup>89</sup>Zr, <sup>89</sup>Zr was produced at Mianyang Central Hospital on the Jiuyuan 11-MTS cyclotron (Longevous Beamtech, China) and isolated with the automated separation device (Longevous Beamtech, China). The <sup>89</sup>Zr oxalic acid (1 M oxalic acid, 0.74 MBq/uL) solution (Jiuyuan-11MTS" medical cyclotron

solid target of Si Chuan Longevous Beam Tech CO, LTD) was added to sterilized 1.5mL centrifuge tubes and neutralized to pH 7.0 with 2 M Na<sub>2</sub>CO<sub>3</sub> solution or 0.88 M Na<sub>2</sub>HPO<sub>4</sub> solution and 0.5 μL p-SCN-Bn-DFO solution (20 μmol/μL, Macrocyclics, Inc). This solution was mixed for 60 min at 37 °C. After the reaction, 1 uL aliquots were spotted on the origin of iTLC-SG (Agilent, SGI0001) plate (2.5 cm above the bottom), which were developed using the mobile phase DTPA (50 mM, pH=5.0). The stability of [<sup>89</sup>Zr]Zr-DFO at 1h, 6h, and 24h was determined by radio-TLC scanner (Eckert & Ziegler, USA), and areas under the curves were analyzed to determine percent radiochemical conversion.

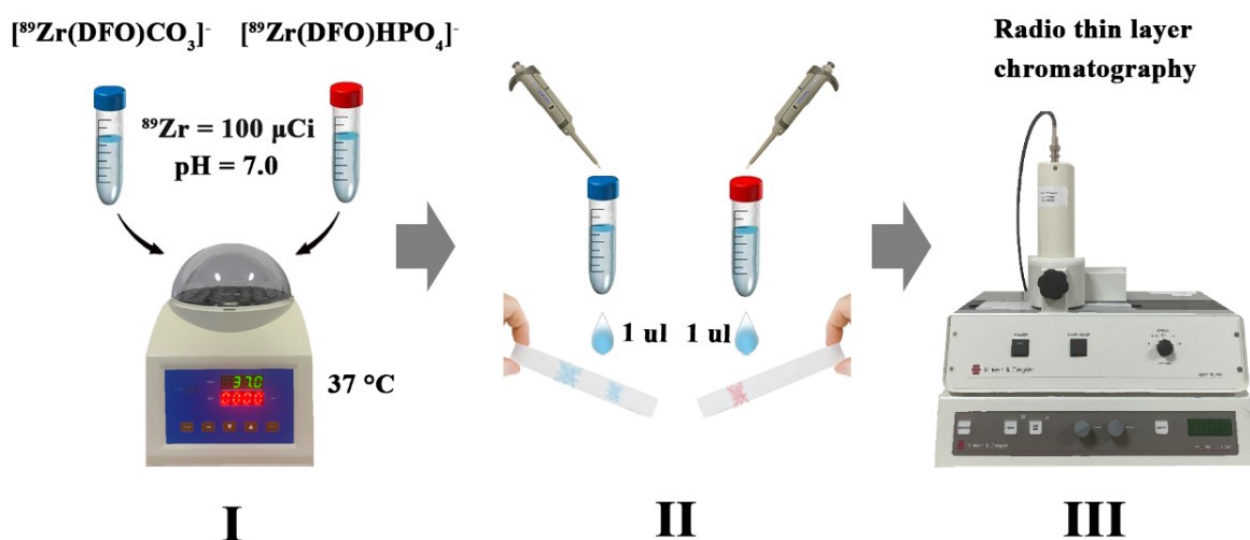


**Figure S1.** Schematic diagram of the flow of <sup>89</sup>Zr-DFO complexation assay.

The partition coefficient of the solute between the mobile phase and the static phase, as determined by a radioactive radio-TLC, is called the retention factor (Rf) value. That is, the ratio of the distance traveled by the solute on the radio-TLC plate from the point of origin to the distance traveled by the mobile phase. The Rf value is calculated as:

$$R_f = \text{Distance traveled (R)} / \text{Mobile phase distance advanced (f)}$$

where the distance traveled refers to the distance reached by the solute moving from the point of origin, and the mobile phase distance advanced refers to the distance reached by the mobile phase moving from the point of departure.

**High-performance liquid chromatography (HPLC).** The Zr<sup>IV</sup> chloride (ZrCl<sub>4</sub>, Macklin, 20 nM) was added to a sterilized centrifuge tube, and the pH was adjusted to approximately 7 using an alkaline

solution ( $\text{Na}_2\text{CO}_3$  and  $\text{Na}_2\text{HPO}_4$ ). After allowing the mixture to stand for 3 minutes, 1  $\mu\text{L}$  of deferoxamine (DFO, Macrocyclics, 20 nM) solution was added and thoroughly mixed. The reaction was then carried out at 37 °C for 60 minutes, with manual shaking every 10 minutes to ensure proper mixing.

After the reaction, the cold reference Zr compounds were obtained. These complexes were analyzed using a HPLC system (Shimadzu), equipped with LabSolutions software, a binary pump, an auto-sampler, a photodiode array detector, a multi-channel fluorescence detector, a column heater, a fraction collector, and a Shim-pack VP-ODS C18 column (5  $\mu\text{m}$ , 4.6  $\times$  100 mm, Thermo Scientific), as well as a B-FC-3100 low-energy gamma probe radiation detector (Eckert & Ziegler, USA). A 10  $\mu\text{L}$  sample of the DFO and Zr compound solution was injected into the system for analysis at 254 nm. The mobile phase consisted of 0.1% TFA in  $\text{H}_2\text{O}$  (Solvent A) and 0.1% TFA in acetonitrile (Solvent B), using a gradient elution from 10% B to 90% B at a flow rate of 1 mL/min.

**In Vitro Stability Study.** The prepared [ $^{89}\text{Zr}$ ]Zr-DFO-ligands complexes (100  $\mu\text{Ci}$ ) were mixed with human serum in equal volume ratios and reacted at 37°C. Samples were then taken for pH measurement and radio-TLC analysis (Eckert & Ziegler, USA) at 1, 6, 24, 48, 72, 96, 120, and 144 h.

**Part 2. Eight possible geometrical isomer structures of Zr<sup>IV</sup>-DFO**

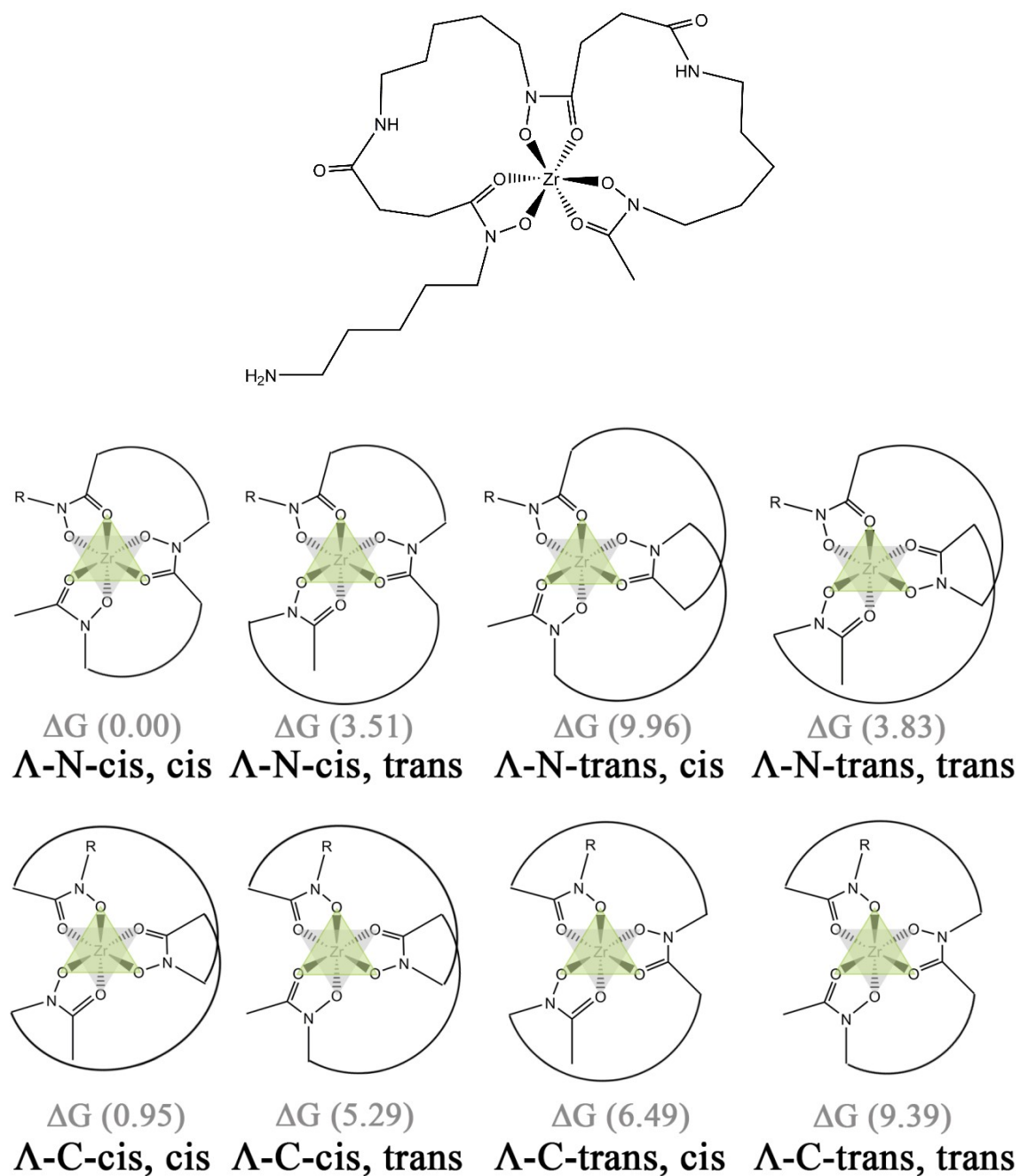


**Figure S2.** The Lewis structure of Zr<sup>IV</sup>-DFO, and the structures of the eight possible geometric isomers when DFO coordinates to the Zr<sup>IV</sup> ion. Note that only structures for the  $\Lambda$ -enantiomers are presented. The nomenclature used to describe each isomer is consistent with that reported by Borgias et al.<sup>20</sup> (unit: kcal/mol)

### Part 3. Optimized geometries of the Zr<sup>IV</sup>-DFO-ligands complexes

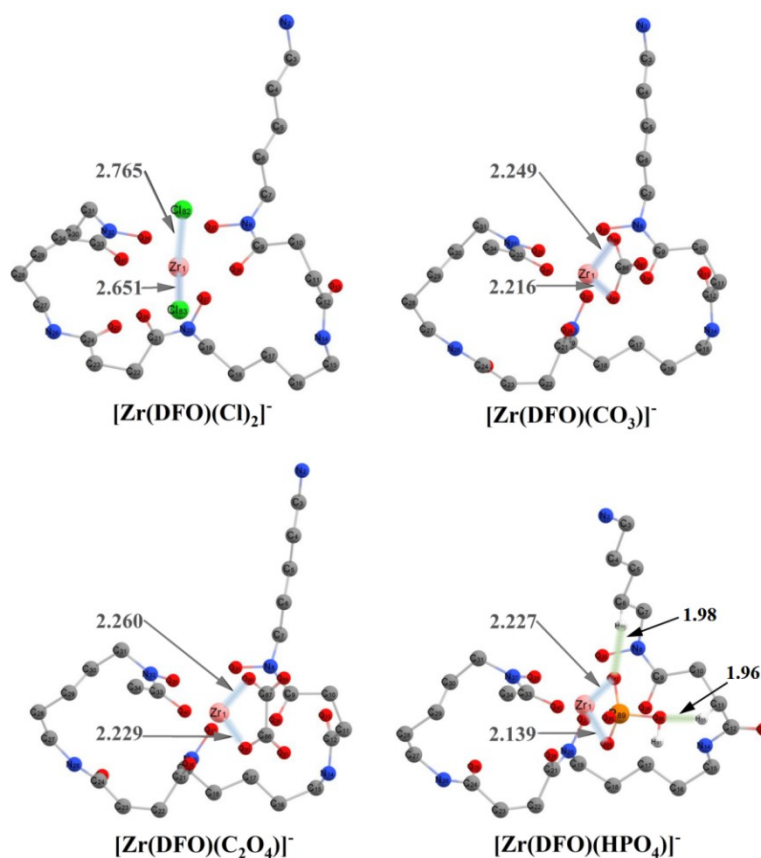


**Figure S3.** Optimized geometries of the octahedral coordinated Zr<sup>IV</sup>-DFO-ligands complexes. The ligands are the Cl<sup>-</sup>, C<sub>2</sub>O<sub>4</sub><sup>2-</sup>, CO<sub>3</sub><sup>2-</sup> and HPO<sub>4</sub><sup>2-</sup> with different reactivity. For the sake of clarity, the hydrogen atoms that do not form hydrogen bonds in DFO are omitted. The characteristic distances ( $d_{\text{Zr-Hapto(ligand)}}$ ) of Zr<sup>IV</sup>-DFO-ligands are given in the figure. (unit: Å)

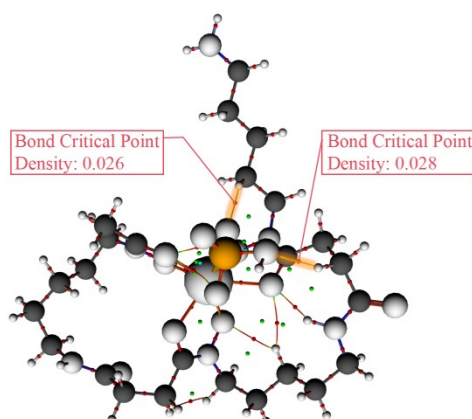


**Figure S4.** Schematic diagram of the bond critical points of hydrogen bonds in the  $[\text{Zr}^{\text{IV}}(\text{DFO})(\text{HPO}_4^{2-})]^-$  complex.

Bond critical points (BCPs) in the quantum theory of atoms in molecules (QTAIM) are defined as the numbers of critical points of different types in a scalar field. As shown in the figure below, the orange highlighted section showing a bond path (BP). The nuclei of the bonded atoms are linked by a line in which the electron density is a maximum with respect to any neighboring lines. The minimum in the electron density (Density: 0.026 and 0.028) along the bond path is the bond critical point (BCP, the red balls). The C-H...O interaction in the highlighted part validates the inference of the presence of hydrogen bonds in the complex from the side.

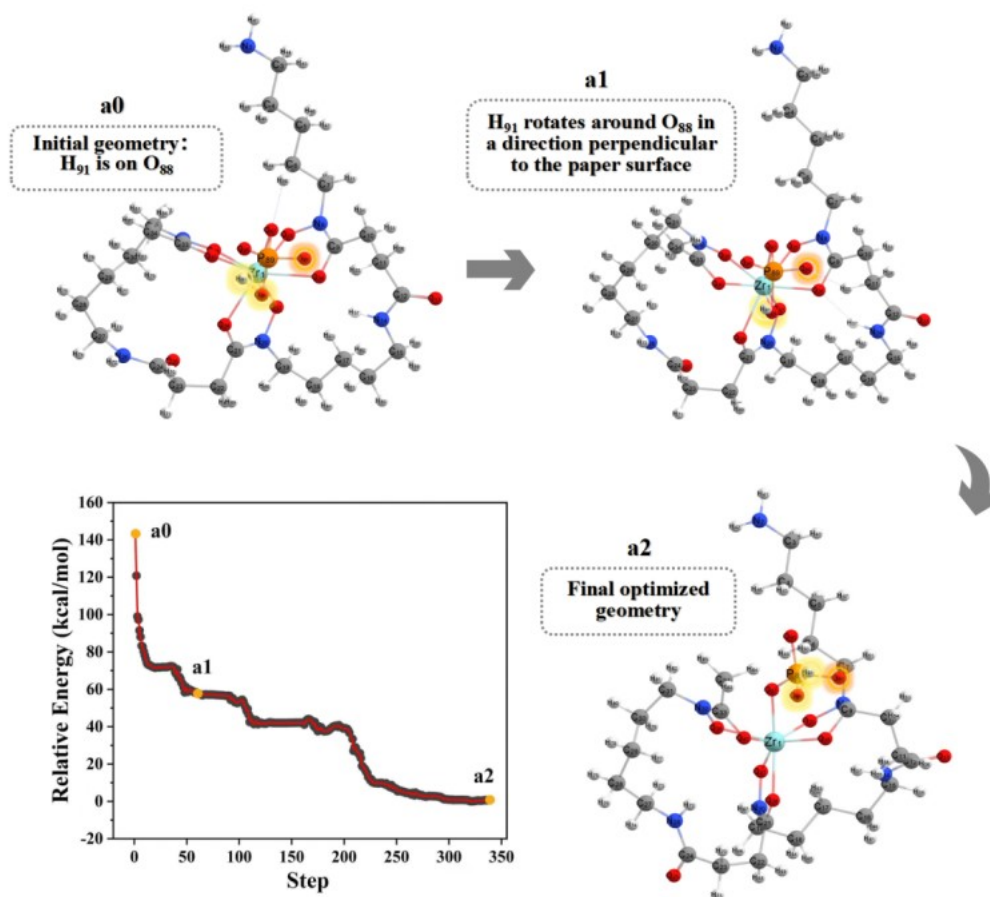


**Figure S5.** Optimized geometry and energy curve of Zr<sup>IV</sup>-DFO-HPO<sub>4</sub><sup>2-</sup> isomer in aqueous solution calculated at PBE-D3/TZ2P levels. (kcal/mol).

As shown in the **Figure S5**, the stereo-ligand HPO<sub>4</sub><sup>2-</sup> may have other coordination sites, i.e., isomers, compared to other planar ligands (Cl<sup>-</sup>, C<sub>2</sub>O<sub>4</sub><sup>2-</sup> and CO<sub>3</sub><sup>2-</sup>). Thus, we have carried out additional calculations to explore the isomers, where H<sub>91</sub> is positioned on O<sub>88</sub> and oriented towards O<sub>40</sub> of DFO (i.e. O<sub>88</sub>-H<sub>91</sub>-O<sub>40</sub>). However, during optimization, the O<sub>88</sub>-H<sub>91</sub>-O<sub>40</sub> bond gradually rotated, and the hydrogen phosphate ion began to disengage from the Zr<sup>IV</sup>-DFO complex. Our calculations indicate

that the isomer does not lead to a stable configuration under the current coordination environment due to electrostatic repulsion and steric hindrance. The detachment tendency of the  $\text{HPO}_4^{2-}$  ligand leads to a "vacant" region around the  $\text{Zr}^{\text{IV}}$  ion, which could compromise the overall stability of the complex. For these reasons, we did not consider this configuration as the primary model for our study.

## Part 4. Geometric parameters of Zr<sup>IV</sup>-DFO-ligands complexes

**Table S1.** Characteristic average distances (in Å) for Zr<sup>IV</sup>-DFO-ligands complexes. See **Figure 1b** for the details of the bond length.

Geometries	[Zr <sup>IV</sup> (DFO) ( <sup>in</sup> H <sub>2</sub> O)( <sup>out</sup> H <sub>2</sub> O)] <sup>+</sup>	[Zr <sup>IV</sup> (DFO)(Cl) <sub>2</sub> ] <sup>-</sup>	[Zr <sup>IV</sup> (DFO) (C <sub>2</sub> O <sub>4</sub> ) <sup>-</sup>	[Zr <sup>IV</sup> (DFO) (CO <sub>3</sub> ) <sup>-</sup>	[Zr <sup>IV</sup> (DFO) (HPO <sub>4</sub> ) <sup>-</sup>	[Zr <sup>IV</sup> (DFO)] <sup>+</sup>
<i>d</i> <sub>Zr-O(DFO)</sub>	2.154	2.187	2.186	2.172	2.151	2.080
<i>d</i> <sub>Zr-O(DFO)</sub>	2.188	2.251	2.262	2.285	2.308	2.161
<i>d</i> <sub>Zr-O(DFO)</sub>	2.107	2.142	2.189	2.203	2.167	2.084
<i>d</i> <sub>Zr-O(DFO)</sub>	2.160	2.274	2.237	2.229	2.254	2.156
<i>d</i> <sub>Zr-O(DFO)</sub>	2.127	2.146	2.150	2.167	2.143	2.076
<i>d</i> <sub>Zr-O(DFO)</sub>	2.172	2.263	2.280	2.284	2.223	2.168
<i>d</i> <sub>average(DFO)</sub>	<b>2.151</b>	<b>2.210</b>	<b>2.217</b>	<b>2.224</b>	<b>2.208</b>	<b>2.121</b>
<i>d</i> <sub>Zr-Hapto(ligand)</sub>	3.942	2.765	2.260	2.249	2.227	/
<i>d</i> <sub>Zr-Hapto(ligand)</sub>	2.334	2.651	2.229	2.216	2.139	/
<i>d</i> <sub>average(ligand)</sub>	/	<b>2.708</b>	<b>2.245</b>	<b>2.233</b>	<b>2.183</b>	/

**Table S2.** Twist angles (in °) for Zr<sup>IV</sup>-DFO-ligands complexes. See **Figure 1b** for the details of the torsion angles.

Geometries	[Zr <sup>IV</sup> (DFO) ( <sup>in</sup> H <sub>2</sub> O)( <sup>out</sup> H <sub>2</sub> O)] <sup>+</sup>	[Zr <sup>IV</sup> (DFO)(Cl) <sub>2</sub> ] <sup>-</sup>	[Zr <sup>IV</sup> (DFO) (C <sub>2</sub> O <sub>4</sub> ) <sup>-</sup>	[Zr <sup>IV</sup> (DFO) (CO <sub>3</sub> ) <sup>-</sup>	[Zr <sup>IV</sup> (DFO) (HPO <sub>4</sub> ) <sup>-</sup>	[Zr <sup>IV</sup> (DFO)] <sup>+</sup>
$\omega_1/\omega_1'$	96.4	127.3	126.6	122.9	122.3	113.4
$\omega_2/\omega_2'$	116.4	126.0	111.5	105.5	118.1	91.9

## Part 5. Comparison of Structural Parameters

We report a summary of structural parameters for the Zr<sup>IV</sup>-DFO complex and its derivatives (**Table S3**) to verify the reliability of our results. For Zr<sup>IV</sup>-DFO, consistent conclusions were obtained using the PBE functional in aqueous solution, which also closely matched the PBE results under gas-phase conditions. Additionally, we compared the octadentate complexes of Zr<sup>IV</sup>-DFO and its derivatives, which were obtained in the experimental and theoretical environments, respectively. We also find that the Zr<sup>IV</sup> ion is usually stable under octagonal coordination due to its ionic radius, which supports the rationality of an octagonal structure. In addition, the reliability of our method can be confirmed by comparing with previous data of Zr<sup>IV</sup>-DFO.

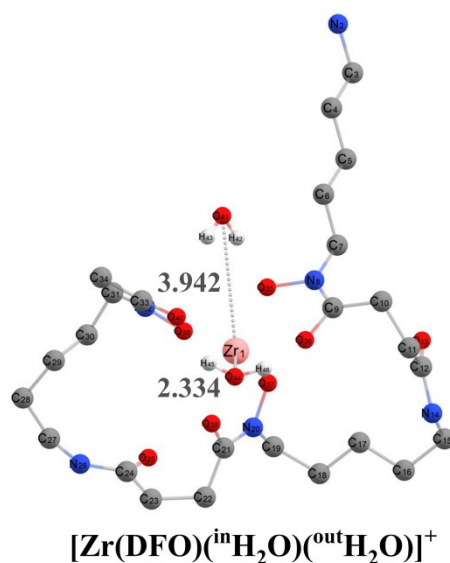
**Table S3.** Summary of structural parameters for the Zr<sup>IV</sup>-DFO complex and its derivatives.

Geometries	$d_{Zr-O(C)}$	$d_{Zr-O(N)}$	$d_{Zr-X(ligands)}$	Technique	References
[Zr <sup>IV</sup> (DFO)] <sup>+</sup> (CN=6)	2.162	2.080	/	PBE/TZ2P with COSMO	Our work
	2.185	2.112	/	PBE/DND with COSMO	Ref [2]
[Zr <sup>IV</sup> (DFO)] <sup>+</sup> (CN=7)	2.282	2.188	2.099 (N)	PBE/DND with COSMO	Ref [2]
[Zr <sup>IV</sup> (HDFO)] <sup>2+</sup>	2.177	2.085	/	B3LYP/6-31+G(d) and LANL2DZ (gas phase)	Ref [21]
[Zr <sup>IV</sup> (DFO)( <sup>in</sup> H <sub>2</sub> O)( <sup>out</sup> H <sub>2</sub> O)] <sup>+</sup>	2.173	2.129	2.334	PBE/TZ2P with COSMO	Our work
[Zr <sup>IV</sup> (DFO)(H <sub>2</sub> O)] <sup>+</sup>	2.213	2.125	2.365	PBE/DND with COSMO	Ref [2]
[Zr <sup>IV</sup> (HDFO)(H <sub>2</sub> O)] <sup>2+</sup> -ax	2.194	2.118	2.460	B3LYP/6-31+G(d) and LANL2DZ (gas phase)	Ref [21]
[Zr <sup>IV</sup> (HDFO)(H <sub>2</sub> O)] <sup>2+</sup> -eq	2.212	2.115	2.362	B3LYP/6-31+G(d) and LANL2DZ (gas phase)	Ref [21]
[Zr <sup>IV</sup> (HDFO)(H <sub>2</sub> O)] <sup>2+</sup> -cis	2.233	2.143	2.400	B3LYP/6-31+G(d) and LANL2DZ (gas phase)	Ref [21]
[Zr <sup>IV</sup> (DFO)(H <sub>2</sub> O) <sub>2</sub> ] <sup>+</sup> -trans	2.255	2.152	2.385	PBE/DND with COSMO	Ref [2]
[Zr <sup>IV</sup> (DFO)(H <sub>2</sub> O) <sub>2</sub> ] <sup>+</sup> -cis	2.232	2.17	2.390	PBE/DND with COSMO	Ref [2]
[Zr <sup>IV</sup> DFO(H <sub>2</sub> O) <sub>2</sub> ] <sup>2+</sup> -with nonhydrogen bonded amine group	2.257	2.178	/	B3LYP/CEP-121G with CPCM	Ref [22]
[Zr <sup>IV</sup> DFO(H <sub>2</sub> O) <sub>2</sub> ] <sup>2+</sup> -with hydrogen bonded amine group	2.260	2.176	/	B3LYP/CEP-121G (gas phase)	Ref [22]
Zr <sup>IV</sup> (DFO)(OH)	2.263	2.177	2.205	PBE/DND with COSMO	Ref [2]
Zr <sup>IV</sup> (DFO)(H <sub>2</sub> O)(OH)-trans	2.328	2.186	2.300	PBE/DND with COSMO	Ref [2]
Zr <sup>IV</sup> (DFO)(H <sub>2</sub> O)(OH)-cis	2.304	2.192	2.400	PBE/DND with COSMO	Ref [2]
[Zr <sup>IV</sup> (DFO)(OH) <sub>2</sub> ] <sup>-</sup> -trans	2.385	2.242	2.108	PBE/DND with COSMO	Ref [2]
[Zr <sup>IV</sup> (DFO)(OH) <sub>2</sub> ] <sup>-</sup> -cis	2.385	2.245	2.112	PBE/DND with COSMO	Ref [2]

<b>[Zr<sup>IV</sup>(DFO)(OH)<sub>2</sub>]<sup>-</sup></b>	2.384	2.338	/	B3LYP/CEP-121G with CPCM	Ref [22]
<b>[Zr<sup>IV</sup>(DFO)(Cl)<sub>2</sub>]<sup>-</sup></b>	2.263	2.158	2.708	PBE/TZ2P with COSMO	Our work
<b>[Zr<sup>IV</sup>(DFO)(CO<sub>3</sub>)<sup>-</sup>]</b>	2.266	2.181	2.224	PBE/TZ2P with COSMO	Our work
<b>[Zr<sup>IV</sup>(DFO)(C<sub>2</sub>O<sub>4</sub>)<sup>-</sup>]</b>	2.260	2.175	2.217	PBE/TZ2P with COSMO	Our work
<b>[Zr<sup>IV</sup>(DFO)(HPO<sub>4</sub>)<sup>-</sup>]</b>	2.262	2.154	2.183	PBE/TZ2P with COSMO	Our work
	2.206	2.188	/	Single-crystal X-ray diffraction data	Ref [23]
<b>Zr<sup>IV</sup>(HOPO)</b>	2.209	2.268	/	PBE/DND with COSMO	Ref [2]
	2.293	2.175	/	B3LYP/ LACVP (gas phase)	Ref [24]
	2.190	2.190	/	Single-crystal X-ray diffraction data	Ref [25]
<b>Zr<sup>IV</sup>(Me-AHA)<sub>4</sub></b>	2.320	2.200	/	B3LYP/DGDZVP	Ref [25]
	2.270	2.200	/	PBE/DND with COSMO	Ref [2]
<b>Zr<sup>IV</sup>(AHA)<sub>4</sub></b>	2.200	2.300	/	PBE/DND with COSMO	Ref [2]
	2.168	2.212	/	Single-crystal X-ray diffraction data	Ref [26]
<b>Zr<sup>IV</sup>(3,2-HOPO)<sub>4</sub></b>	2.203	2.244	/	PBE/DND with COSMO	Ref [2]
	2.209	2.191	/	Single-crystal X-ray diffraction data	Ref [27]
<b>Zr<sup>IV</sup>(1,2-PIPOH)<sub>4</sub></b>	2.137	2.348	/	PBE/DND with COSMO	Ref [2]
<b>Zr<sup>IV</sup>-DFO2</b>	2.260	2.220	/	PBE/DND with COSMO	Ref [3]
<b>Zr<sup>IV</sup>-DFO2p</b>	2.28	2.210	/	PBE/DND with COSMO	Ref [3]

“X” denotes the atoms in contact with Zr<sup>IV</sup> in the ligand.

## Part 6. Optimized geometry of the $[\text{Zr}^{\text{IV}}(\text{DFO})(^{\text{in}}\text{H}_2\text{O})(^{\text{out}}\text{H}_2\text{O})]^+$ complex

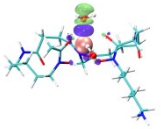
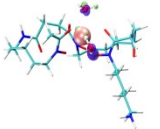
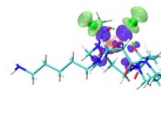
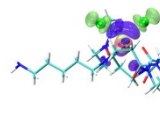
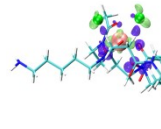
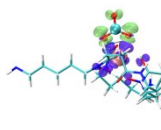
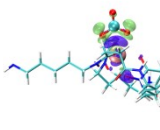
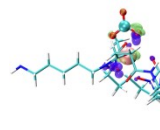
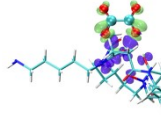
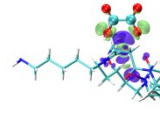
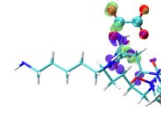
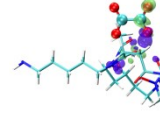
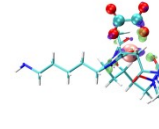
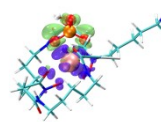
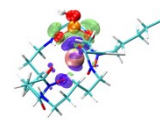
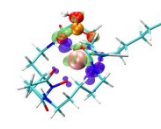
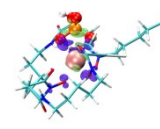
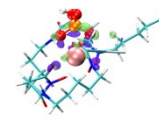


**Figure S6.** Optimized geometry of the  $[\text{Zr}^{\text{IV}}(\text{DFO})(^{\text{in}}\text{H}_2\text{O})(^{\text{out}}\text{H}_2\text{O})]^+$  complex. (unit: Å)

For the monodentate ligand  $\text{H}_2\text{O}$ ,  $^{\text{in}}\text{H}_2\text{O}$  binds to  $[\text{Zr}^{\text{IV}}(\text{DFO})]^+$  complex in synergic coordination site 2, resulting in an increased torsion angle  $\omega_2$  in the corresponding plane. Meanwhile, the four nearest O atoms on DFO in synergic coordination site 2 experience outward expansion due to spatial repulsion, leading to a varying degree of reduction in the torsion angle  $\omega_1$  in the other plane. As a result, the  $^{\text{out}}\text{H}_2\text{O}$  molecule in synergic coordination site 1 exists in a highly ‘loose’ form outside the complex. The reason behind this could be attributed to the increased electron density caused by the binding of a water molecule in  $[\text{Zr}^{\text{IV}}(\text{DFO})(^{\text{in}}\text{H}_2\text{O})]^+$ , which repels the entry of a second water molecule.<sup>28</sup> Previous calculations have also indicated that the structure formed by a water molecule in synergic coordination 2 as an auxiliary ligand is more stable than in synergic coordination site 1.<sup>2</sup> Hence, in our study, the  $[\text{Zr}^{\text{IV}}(\text{DFO})(^{\text{in}}\text{H}_2\text{O})(^{\text{out}}\text{H}_2\text{O})]^+$  complex with water molecule as auxiliary ligands exists in a dynamic 7-/8-coordination. Furthermore, it has also been observed that when  $\text{Zr}^{\text{IV}}\text{-DFO}$  binds to  $\text{H}^+$  in the solvent to form  $\text{Zr}^{\text{IV}}\text{-HDFO}$  complex, two  $\text{H}_2\text{O}$  molecules can form an octahedral coordination complex through structural relaxation induced by ligand coordination, which has been reported in previous studies.<sup>21, 29</sup>

## Part 7. EDA-NOCV deformation densities $\Delta\rho$ of $\text{Zr}^{\text{IV}}$ -DFO-ligands complex

**Table S4.** Plots of the EDA-NOCV deformation densities  $\Delta\rho$  (isovalue = 0.0015) of the pairwise orbital interactions and the associated fragment molecular orbitals for the different forms of interacting fragments in aqueous solution at the PBE-D3/TZ2P level of theory. The corresponding energy values are given in table (kcal/mol). The direction of the charge flow is green  $\rightarrow$  purple.

Geometries	$\Delta\rho_1$	$\Delta\rho_2$	$\Delta\rho_3$	$\Delta\rho_4$	$\Delta\rho_5$
$[\text{Zr}^{\text{IV}}(\text{DFO})(^{\text{in}}\text{H}_2\text{O})(^{\text{out}}\text{H}_2\text{O})]^+$	 -15.64	 -3.49	 -2.70	/	/
$[\text{Zr}^{\text{IV}}(\text{DFO})(\text{Cl})_2]^-$	 -29.59	 -19.60	 -11.36	/	/
$[\text{Zr}^{\text{IV}}(\text{DFO})(\text{CO}_3)]^-$	 -46.02	 -30.83	 -13.03	 -10.77	/
$[\text{Zr}^{\text{IV}}(\text{DFO})(\text{C}_2\text{O}_4)]^-$	 -36.38	 -27.20	 -9.68	 -9.14	 -5.85
$\text{Zr}^{\text{IV}}(\text{DFO})(\text{HPO}_4)]^-$	 -45.74	 -30.65	 -12.85	 -11.61	 -9.55

The EDA-NOCV calculations allow for a further breakdown of  $\Delta E_{\text{orb}}$  into pairwise orbital interactions. When we divided the complex into two fragments,  $\text{Zr}^{\text{IV}}$ -DFO and auxiliary ligand, the interaction strength between the fragments will be determined not only by  $\Delta E_{\text{int}}$  but also by the balance between attractive forces ( $\Delta E_{\text{elstat}}$ ,  $\Delta E_{\text{orb}}$ ,  $\Delta E_{\text{dis}}$ ) and the repulsive exchange ( $\Delta E_{\text{Pauli}}$ ) term. Here, the charge flowing direction (green  $\rightarrow$  purple) is always donated to  $\text{Zr}^{\text{IV}}$ -DFO by the auxiliary ligand. **Table S4** present the numerical results, charge flow, and contributing fragment molecular orbitals. For

the Zr-O bond in  $[\text{Zr}^{\text{IV}}(\text{DFO})(^{\text{in}}\text{H}_2\text{O})(^{\text{out}}\text{H}_2\text{O})]^+$ , the crucial  $\Delta E_{\text{orb}(1)}$  (-15.64 kcal/mol, i.e.  $\Delta\rho_1$ ) is primarily donation from the 2p orbital of oxygen to the 4d orbital of Zr. Additionally, a weak interaction between the oxygen of the  $^{\text{out}}\text{H}_2\text{O}$  and H in the  $\text{Zr}^{\text{IV}}\text{-DFO}$  fragment leads to charge flow in  $\Delta E_{\text{orb}(2)}$  from  $\text{Zr}^{\text{IV}}\text{-DFO}$  to  $^{\text{out}}\text{H}_2\text{O}$ . In contrast to water, for the other auxiliary ligands,  $\Delta\rho_1$  primarily involves the donation of electrons from the non-bonding molecular orbitals (NBMO) to the 4d/5s shell orbitals of  $\text{Zr}^{\text{IV}}$  (i.e.,  $\text{NBMO} \rightarrow 4\text{d}/5\text{s}$ ). This suggests weakened interactions within the auxiliary ligands, making them more prone to  $\text{Zr}^{\text{IV}}$  binding. For  $\Delta\rho_2$ , the interaction involves  $\pi$  bonding  $\rightarrow 4\text{d}/5\text{s}/5\text{p}$ .

**Table S5.** EDA-NOCV results (kcal/mol) for the different forms of interacting fragments (gas phase analysis at the solution-optimized geometries), taking  $2\text{H}_2\text{O}$ ,  $2\text{Cl}^-$ ,  $\text{C}_2\text{O}_4^{2-}$ ,  $\text{CO}_3^{2-}$ ,  $\text{HPO}_4^{2-}$  and  $\text{Zr}^{\text{IV}}\text{-DFO}$  in the singlet state as interacting fragments at the corresponding frozen  $\text{Zr}^{\text{IV}}\text{-DFO}$ -ligand geometries.

Energy	$[\text{Zr}^{\text{IV}}(\text{DFO})(\text{CO}_3)]^-$	$[\text{Zr}^{\text{IV}}(\text{DFO})(\text{C}_2\text{O}_4)]^-$	$[\text{Zr}^{\text{IV}}(\text{DFO})(\text{HPO}_4)]^-$	$[\text{Zr}^{\text{IV}}(\text{DFO})(\text{Cl})_2]^-$	$[\text{Zr}^{\text{IV}}(\text{DFO})(^{\text{in}}\text{H}_2\text{O})(^{\text{out}}\text{H}_2\text{O})]^+$
$\Delta E_{\text{int}}$	-288.72	-251.93	-238.18	-232.17	-28.79
$\Delta E_{\text{Pauli}}$	150.85	130.98	295.81	102.50	57.40
$^{\text{a}}\Delta E_{\text{dis}}$	-3.35 (0.76%)	-4.46 (1.16%)	-8.19 (1.53%)	-4.37 (1.31%)	-5.42 (6.29%)
$^{\text{a}}\Delta E_{\text{elstat}}$	-281.96 (64.14%)	-247.90 (64.74%)	-352.57 (66.03%)	-218.58 (65.31%)	-52.26 (60.63%)
$^{\text{a}}\Delta E_{\text{orb}}$	-154.27 (35.10%)	-130.55 (34.09%)	-173.23 (32.44%)	-111.72 (33.38%)	-28.51 (33.08%)
$^{\text{b}}\Delta E_{\text{orb}(1)}$	-46.02 (29.83%) [ $\text{CO}_3^{2-} \rightarrow \text{Zr}_{4\text{d}+5\text{s}+5\text{p}}$ ]	-36.38 (27.87%) [ $\text{C}_2\text{O}_4^{2-} \rightarrow \text{Zr}_{4\text{d}}$ ]	-45.74 (26.4%) [ $\text{HPO}_4^{2-} \rightarrow \text{Zr}_{4\text{d}}$ ]	-29.59 (26.49%) [ $\text{Cl}^- \rightarrow \text{Zr}_{4\text{d}+5\text{s}}$ ]	-15.64 (54.86%) [ $^{\text{in}}\text{H}_2\text{O} \rightarrow \text{Zr}_{4\text{d}}$ ]
$^{\text{b}}\Delta E_{\text{orb}(2)}$	-30.83 (19.98%) [ $\text{CO}_3^{2-} \rightarrow \text{Zr}_{4\text{d}+5\text{s}+5\text{p}}$ ]	-27.20 (20.83%) [ $\text{C}_2\text{O}_4^{2-} \rightarrow \text{Zr}_{4\text{d}}$ ]	-30.65 (17.69%) [ $\text{HPO}_4^{2-} \rightarrow \text{Zr}_{4\text{d}}$ ]	-19.60 (17.54%) [ $\text{Cl}^- \rightarrow \text{Zr}_{4\text{d}+5\text{p}}$ ]	-3.49 (12.24%) [ $\text{Zr}^{\text{IV}}(\text{DFO}) \rightarrow ^{\text{out}}\text{H}_2\text{O}$ ]
$^{\text{b}}\Delta E_{\text{orb}(3)}$	-13.03 (8.45%) [ $\text{CO}_3^{2-} \rightarrow \text{Zr}_{4\text{d}+5\text{s}}$ ]	-9.68 (7.41%) [ $\text{C}_2\text{O}_4^{2-} \rightarrow \text{Zr}_{4\text{d}+5\text{s}}$ ]	-12.85 (7.42%) [ $\text{HPO}_4^{2-} \rightarrow \text{Zr}_{4\text{d}}$ ]	-11.36 (10.17%) [ $\text{Cl}^- \rightarrow \text{Zr}_{4\text{d}+5\text{s}}$ ]	-2.70 (9.47%) [ $^{\text{in}}\text{H}_2\text{O} \rightarrow ^{\text{in}}\text{H}_2\text{O}$ ]
$^{\text{b}}\Delta E_{\text{orb}(4)}$	-10.77 (6.98%) [ $\text{CO}_3^{2-} \rightarrow \text{Zr}_{4\text{d}+5\text{s}}$ ]	-9.14 (7.00%) [ $\text{C}_2\text{O}_4^{2-} \rightarrow \text{Zr}_{4\text{d}+5\text{s}}$ ]	-11.61 (6.70%) [ $\text{HPO}_4^{2-} \rightarrow \text{Zr}^{\text{IV}}(\text{DFO})$ ]	-51.17 (45.80%) [rest: polarization]	-6.68 (23.43%) [rest: polarization]
$^{\text{b}}\Delta E_{\text{orb}(5)}$	-53.62 (34.76%) [rest: polarization]	-5.85 (4.48%) [ $\text{C}_2\text{O}_4^{2-} \rightarrow \text{Zr}_{4\text{d}+5\text{s}}$ ]	-9.55 (5.51%) [ $\text{HPO}_4^{2-} \rightarrow \text{Zr}^{\text{IV}}(\text{DFO})$ ]	/	/
$^{\text{b}}\Delta E_{\text{orb}(6)}$	/	42.30 (32.40) [rest: polarization]	62.83 (36.27%) [rest: polarization]	/	/

a: The value in parentheses gives the percentage contribution to the total attractive interactions  $\Delta E_{\text{elstat}} + \Delta E_{\text{orb}} + \Delta E_{\text{dis}}$ ; b:

Values in parentheses give the percentage of each attractive term with respect to the  $\Delta E_{\text{orb}}$  term.

## Part 8. Stability Constants and Gibbs free energy

**Table S6.** Stability Constants and Gibbs free energy for various Zr<sup>IV</sup>-DFO complexes in aqueous solution obtained at PBE-D3/TZ2P levels (kcal/mol).

Metal Ligand Complexation Reaction	Reaction Gibbs Free Energy (Δ <sub>r</sub> G)	Stability Constant (logβ)
$[\text{Zr}^{\text{IV}}(\text{H}_2\text{O})_8]^{4+} + [\text{DFO}]^{3-} \rightleftharpoons [\text{Zr}^{\text{IV}}(\text{DFO})]^+ + 8\text{H}_2\text{O}$	-198.77	145.79
$[\text{Zr}^{\text{IV}}(\text{H}_2\text{O})_8]^{4+} + [\text{DFO}]^{3-} + 2\text{H}_2\text{O} \rightleftharpoons [\text{Zr}^{\text{IV}}(\text{DFO})(^{\text{in}}\text{H}_2\text{O})(^{\text{out}}\text{H}_2\text{O})]^+ + 8\text{H}_2\text{O}$	-199.07	146.01
$[\text{Zr}^{\text{IV}}(\text{H}_2\text{O})_8]^{4+} + [\text{DFO}]^{3-} + 2\text{Cl}^- \rightleftharpoons [\text{Zr}^{\text{IV}}(\text{DFO})(\text{Cl})_2]^- + 8\text{H}_2\text{O}$	-212.72	156.02
$[\text{Zr}^{\text{IV}}(\text{H}_2\text{O})_8]^{4+} + [\text{DFO}]^{3-} + \text{C}_2\text{O}_4^{2-} \rightleftharpoons [\text{Zr}^{\text{IV}}(\text{DFO})(\text{C}_2\text{O}_4^{2-})]^- + 8\text{H}_2\text{O}$	-219.42	160.94
$[\text{Zr}^{\text{IV}}(\text{H}_2\text{O})_8]^{4+} + [\text{DFO}]^{3-} + \text{CO}_3^{2-} \rightleftharpoons [\text{Zr}^{\text{IV}}(\text{DFO})(\text{CO}_3^{2-})]^- + 8\text{H}_2\text{O}$	-224.12	164.39
$[\text{Zr}^{\text{IV}}(\text{H}_2\text{O})_8]^{4+} + [\text{DFO}]^{3-} + \text{HPO}_4^{2-} \rightleftharpoons [\text{Zr}^{\text{IV}}(\text{DFO})(\text{HPO}_4^{2-})]^- + 8\text{H}_2\text{O}$	-306.75	224.99

**Part 9. The radiochemical purity of purified  $^{89}\text{Zr}$**

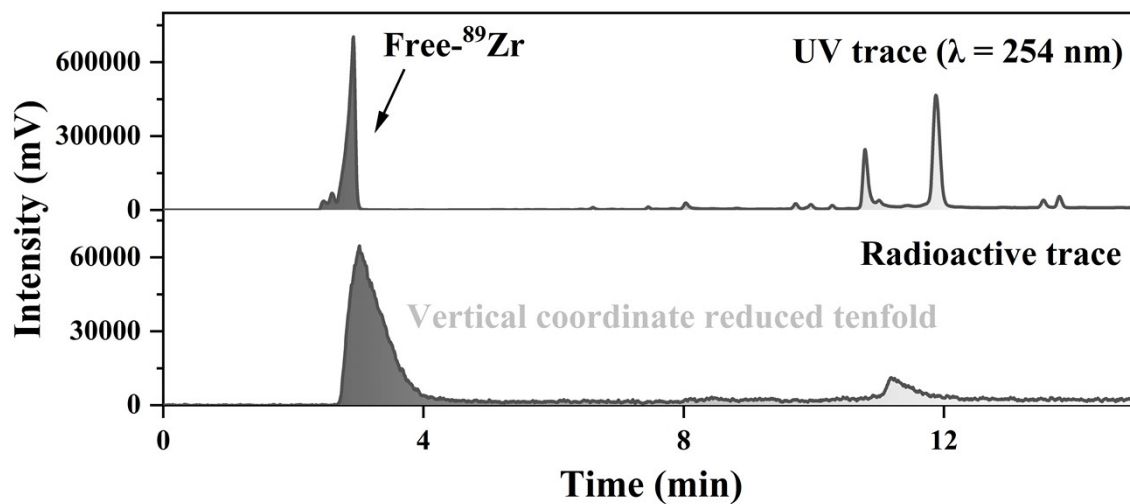


**Figure S7.** Radio-high-performance liquid chromatography (Radio-HPLC) results of  $^{89}\text{Zr}$ .

## Part 10. In vitro stability of [<sup>89</sup>Zr]Zr-DFO and [<sup>89</sup>Zr]Zr-DFO-ligands

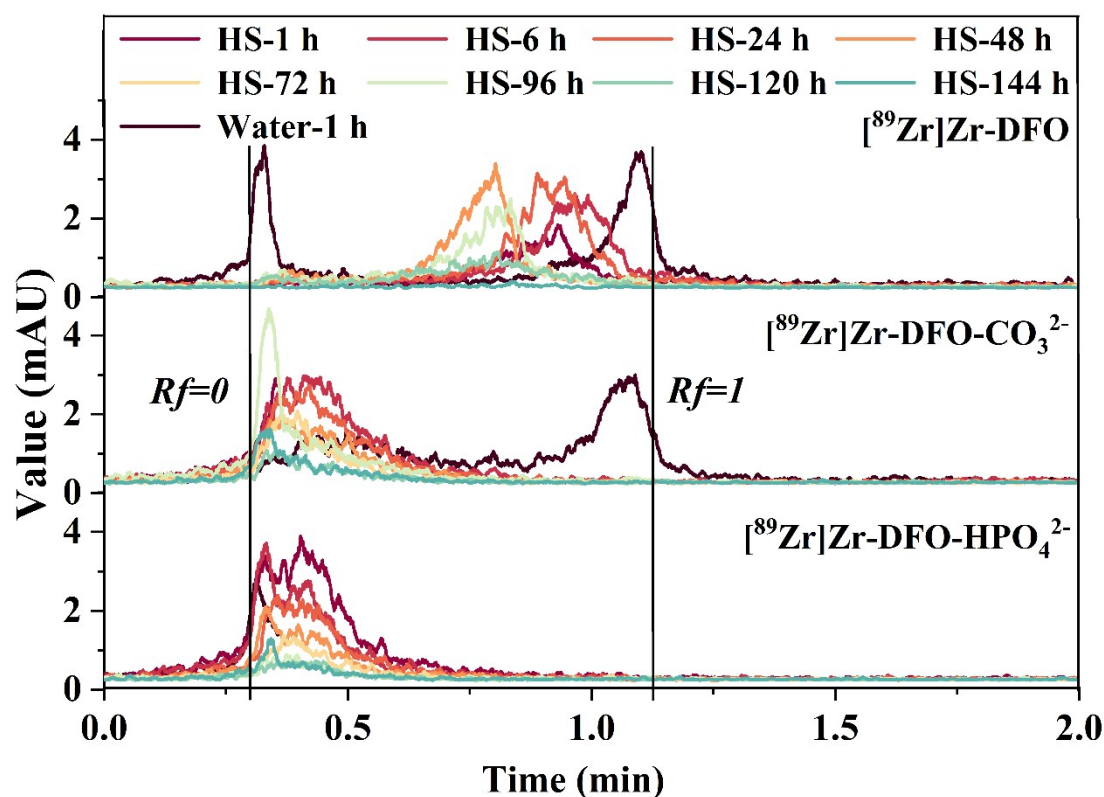


**Figure S8.** Human Serum in vitro stability of [<sup>89</sup>Zr]Zr-DFO-HPO<sub>4</sub><sup>2-</sup>, [<sup>89</sup>Zr]Zr-DFO-CO<sub>3</sub><sup>2-</sup> and [<sup>89</sup>Zr]Zr-DFO, monitored by Radio-TLC. The complexes were incubated at 37°C for 144 h. [<sup>89</sup>Zr]Zr-DFO-HPO<sub>4</sub><sup>2-</sup> in human serum at pH 7; [<sup>89</sup>Zr]Zr-DFO-CO<sub>3</sub><sup>2-</sup> in human serum at pH 8; [<sup>89</sup>Zr]Zr-DFO in human serum at pH 1. The retention times of the three are indicated.

To measure the in vitro stability of [<sup>89</sup>Zr]Zr-DFO-HPO<sub>4</sub><sup>2-</sup>, [<sup>89</sup>Zr]Zr-DFO-CO<sub>3</sub><sup>2-</sup>, and [<sup>89</sup>Zr]Zr-DFO, samples containing 100 μCi were incubated in freshly prepared human serum (1:1 dilution). Aliquots were taken at various time points (1, 6, 24, 48, 72, 96, 120, and 144 hours) at 37°C and analyzed by Radio-TLC. Radio-TLC analysis revealed that the [<sup>89</sup>Zr]Zr-DFO-HPO<sub>4</sub><sup>2-</sup>, [<sup>89</sup>Zr]Zr-DFO-CO<sub>3</sub><sup>2-</sup> complexes maintained their radiolabeling intact after 24 h of incubation in human serum (**Figure S8**). In contrast, the reference complex [<sup>89</sup>Zr]Zr-DFO exhibited an eluting radioactivity signature at 1 h ( $R_f \approx 1$ ). The incubation pattern of the auxiliary ligands with [<sup>89</sup>Zr]Zr-DFO in human serum was found to be very similar to that of the reference complex, with the only difference being the pH of the three complexes after incubation. Under these conditions, the radiolabeling of the complexes

containing the auxiliary ligands remained stable up to day 7, while the radiolabeling of [<sup>89</sup>Zr]Zr-DFO alone was almost undetectable. These results indicate that the stability of [<sup>89</sup>Zr]Zr-DFO-ligands in serum protein was stronger than the [<sup>89</sup>Zr]Zr-DFO.

## Part 11. References

- (1) Perdew, J. P.; Burke, K.; Ernzerhof, M. Generalized Gradient Approximation Made Simple. *Phys. Rev. Lett.* **1996**, *77*, 3865-3868.
- (2) Summers, K. L.; Sarbisheh, E. K.; Zimmerling, A.; Cotelesage, J. J. H.; Pickering, I. J.; George, G. N.; Price, E. W. Structural characterization of the solution chemistry of zirconium(IV) desferrioxamine: A coordination sphere completed by hydroxides. *Inorg. Chem.* **2020**, *59*, 17443-17452.
- (3) Khozeimeh Sarbisheh, E.; Summers, K. L.; Salih, A. K.; Cotelesage, J. J. H.; Zimmerling, A.; Pickering, I. J.; George, G. N.; Price, E. W. Radiochemical, computational, and spectroscopic evaluation of high-denticity desferrioxamine derivatives DFO2 and DFO2p toward an ideal zirconium-89 chelate platform. *Inorg. Chem.* **2023**, *62*, 2637-2651.
- (4) Grimme, S.; Antony, J.; Ehrlich, S.; Krieg, H. A consistent and accurate ab initio parametrization of density functional dispersion correction (DFT-D) for the 94 elements H-Pu. *J. Chem. Phys.* **2010**, *132*, 154104.
- (5) Van Lenthe, E.; Baerends, E. J. Optimized Slater-type basis sets for the elements 1-118. *J. Comput. Chem.* **2003**, *24*, 1142-1156.
- (6) van Lenthe, E.; Ehlers, A.; Baerends, E.-J. Geometry optimizations in the zero order regular approximation for relativistic effects. *J. Chem. Phys.* **1999**, *110*, 8943-8953.
- (7) van Lenthe, E.; van Leeuwen, R.; Baerends, E. J.; Snijders, J. G. Relativistic regular two-component Hamiltonians. *Int. J. Quantum Chem* **1996**, *57*, 281-293.
- (8) van Lenthe, E.; Snijders, J. G.; Baerends, E. J. The zero-order regular approximation for relativistic effects: The effect of spin-orbit coupling in closed shell molecules. *J. Chem. Phys.* **1996**, *105*, 6505-6516.
- (9) van Lenthe, E.; Baerends, E. J.; Snijders, J. G. Relativistic total energy using regular approximations. *J. Chem. Phys.* **1994**, *101*, 9783-9792.
- (10) Klamt, A.; Schüürmann, G. COSMO: a new approach to dielectric screening in solvents with explicit expressions for the screening energy and its gradient. *J. Chem. Soc., Perkin Trans. 2* **1993**, 799-805.

- (11) Klamt, A. Conductor-like Screening Model for Real Solvents: A New Approach to the Quantitative Calculation of Solvation Phenomena. *J. Phys. Chem.* **2002**, *99*, 2224-2235.
- (12) Klamt, A.; Jonas, V. Treatment of the outlying charge in continuum solvation models. *J. Chem. Phys.* **1996**, *105*, 9972-9981.
- (13) Pye, C. C.; Ziegler, T. An implementation of the conductor-like screening model of solvation within the Amsterdam density functional package. *Theor Chem Acc* **1999**, *101*, 396-408.
- (14) Martin, R. L.; Hay, P. J.; Pratt, L. R. Hydrolysis of Ferric Ion in Water and Conformational Equilibrium. *J. Phys. Chem. A* **1998**, *102*, 3565-3573.
- (15) Ziegler, T.; Rauk, A. On the calculation of bonding energies by the Hartree Fock Slater method. *Theoret. Chim. Acta* **1977**, *46*, 1-10.
- (16) Mitoraj, M. P.; Michalak, A.; Ziegler, T. On the Nature of the Agostic Bond between Metal Centers and  $\beta$ -Hydrogen Atoms in Alkyl Complexes. An Analysis Based on the Extended Transition State Method and the Natural Orbitals for Chemical Valence Scheme (ETS-NOCV). *Organometallics* **2009**, *28*, 3727-3733.
- (17) Sagan, F.; Mitoraj, M. P. A Kinetic and Potential Energy Contributions to a Chemical Bond from the Charge and Energy Decomposition Scheme of Extended Transition State Natural Orbitals for Chemical Valence. *J. Phys. Chem. A* **2019**, *123*, 4616-4622.
- (18) Ziegler, T.; Rauk, A. On the calculation of bonding energies by the Hartree Fock Slater method. *Theoret. Chim. Acta* **1977**, *46*, 1-10.
- (19) te Velde, G.; Bickelhaupt, F. M.; Baerends, E. J.; Fonseca Guerra, C.; van Gisbergen, S. J. A.; Snijders, J. G.; Ziegler, T. Chemistry with ADF. *J. Comput. Chem.* **2001**, *22*, 931-967.
- (20) Borgias, B.; Hugi, A. D.; Raymond, K. N. Isomerization and solution structures of desferrioxamine B complexes of aluminum(3+) and gallium(3+). *Inorg. Chem.* **2002**, *28*, 3538-3545.
- (21) Holland, J. P.; Divilov, V.; Bander, N. H.; Smith-Jones, P. M.; Larson, S. M.; Lewis, J. S.  $^{89}\text{Zr}$ -DFO-J591 for immunoPET of prostate-specific membrane antigen expression in vivo. *J. Nucl. Med.* **2010**, *51*, 1293-1300.
- (22) Deri, M. A.; Ponnala, S.; Zeglis, B. M.; Pohl, G.; Dannenberg, J. J.; Lewis, J. S.; Francesconi, L. C. Alternative chelator for  $^{89}\text{Zr}$  radiopharmaceuticals: Radiolabeling and evaluation of 3,4,3-(LI-1,2-HOPO). *J. Med. Chem.* **2014**, *57*, 4849-4860.

- (23) Deri, M. A.; Ponnala, S.; Kozlowski, P.; Burton-Pye, B. P.; Cicek, H. T.; Hu, C.; Lewis, J. S.; Francesconi, L. C. *p*-SCN-Bn-HOPO: A Superior Bifunctional Chelator for  $^{89}\text{Zr}$  ImmunoPET. *Bioconjug. Chem.* **2015**, *26*, 2579-2591.
- (24) Allott, L.; Da Pieve, C.; Meyers, J.; Spinks, T.; Ciobota, D. M.; Kramer-Marek, G.; Smith, G. Evaluation of DFO-HOPO as an octadentate chelator for zirconium-89. *Chem. Commun.* **2017**, *53*, 8529-8532.
- (25) Guérard, F.; Lee, Y. S.; Tripier, R.; Szajek, L. P.; Deschamps, J. R.; Brechbiel, M. W. Investigation of Zr(IV) and  $^{89}\text{Zr}$ (IV) complexation with hydroxamates: progress towards designing a better chelator than desferrioxamine B for immuno-PET imaging. *Commun. Chem.* **2013**, *49*, 1002-1004.
- (26) Guérard, F.; Beyler, M.; Lee, Y. S.; Tripier, R.; Gestin, J. F.; Brechbiel, M. W. Investigation of the complexation of  $^{\text{nat}}\text{Zr}(\text{iv})$  and  $^{89}\text{Zr}(\text{iv})$  by hydroxypyridinones for the development of chelators for PET imaging applications. *Dalton Trans.* **2017**, *46*, 4749-4758.
- (27) Jewula, P.; Berthet, J. C.; Chambron, J. C.; Rousselin, Y.; Thuéry, P.; Meyer, M. Synthesis and Structural Study of Tetravalent ( $\text{Zr}^{4+}$ ,  $\text{Hf}^{4+}$ ,  $\text{Ce}^{4+}$ ,  $\text{Th}^{4+}$ ,  $\text{U}^{4+}$ ) Metal Complexes with Cyclic Hydroxamic Acids. *Eur. J. Inorg. Chem.* **2015**, *2015*, 1529-1541.
- (28) Holland, J. P. *The radiochemistry of zirconium*; John Wiley & Sons, Ltd, **2020**.
- (29) Racow, E. E.; Kreinbihl, J. J.; Cosby, A. G.; Yang, Y.; Pandey, A.; Boros, E.; Johnson, C. J. General approach to direct measurement of the hydration state of coordination complexes in the gas phase: Variable temperature mass spectrometry. *J. Am. Chem. Soc.* **2019**, *141*, 14650-14660.